Evaluation of Eddy-Current Distortion and EPI Distortion Corrections in MR Diffusion Imaging using Log-Demons DIR Method

by

Theodore Higgins Arsenault

Graduate Program in Medical Physics
Duke University

Date:_____

Approved:

_____
Fang-Fang Yin, Supervisor

_____
Jim Zheng Chang

_____
Junzo Chino

_____
Oana Craciunescu

Thesis submitted in partial fulfillment of
the requirements for the degree of
Master of Science in the Graduate Program in
Medical Physics in the Graduate School
of Duke University

2020

ABSTRACT

Evaluation of Eddy-Current Distortion and EPI Distortion Corrections in MR Diffusion Imaging using Log-Demons DIR Method

by

Theodore Higgins Arsenault

Graduate Program in Medical Physics
Duke University

Date:_____
Approved:

_____
Fang-Fang Yin, Supervisor

_____
Jim Zheng Chang

_____
Junzo Chino

_____
Oana Craciunescu

An abstract of a thesis submitted in partial fulfillment of the requirements for the degree of Master of Science in the Graduate Program in Medical Physics in the Graduate School of Duke University
2020

Abstract

Purpose: To investigate the feasibility of the Log-Demons deformable image registration (DIR) method to correct eddy current and Echo Planar Imaging (EPI) distortions while preserving diffusion tensor information.

Methods: A phantom MR scan was conducted using a diffusion phantom scan (Diffusion Phantom Model 128, High Precision Devices, Inc) on a clinical 3T scanner. The scan includes a standard T1-weighted scan and a 20-direction diffusion tensor imaging (DTI) scan, which consists of one data set with b=0s/mm^2 and twenty diffusion-weighted data sets with b=1,000s/mm^2. A Log-Demons DIR algorithm was applied to the DTI images for eddy current and EPI distortion correction based on the b=0s/mm^2 and T1 weighted data sets and compared the eddy current and EPI distortion corrections along the phase encoding direction by affine and demons DIR algorithms. The Log-Demons framework is optimized based on both similarity and regularization. The registered images were analyzed using Cross-correlation (CC) and mutual information (MI) to assess the performances of distortion corrections by the DIR methods. Quantitative deviations from the original data after correction were also evaluated using the mean, and root mean square error (RMSE) for thirteen regions of interest in the Apparent Diffusion Coefficient (ADC) and Fractional Anisotropy (FA) maps.

The Log-Demons DIR algorithm was then applied to the MASSIVE dataset, which provides diffusion-weighted volumes divided into four sets with both positive (+) and negative(-) diffusion gradient directions and both AP and PA phase encoding directions. The registered images were analyzed using the mutual information (MI) and the absolute mean difference of two images with opposing gradient directions to assess the performances of distortion corrections by the DIR methods. Images with opposing gradient directions were compared when comparing eddy current distortions and images with opposing phase encoding directions were compared for EPI distortions.

Results: In the phantom study, the MI and CC were improved by 2.15%,0.89%, and 39.39% compared to no correction, and affine, and demons algorithm respectively when correction for eddy current distortions. MI and CC were improved by 8.89%, 9.33%, and 9.20% compared to no correction, and affine, and demons algorithm respectively when correction for EPI distortions. Analysis of the tensor metrics using percent difference and the RMS of the ADC and FA found that the Log-Demons algorithm outperforms the other algorithms in terms of preserving diffusion information.

In the MASSIVE study, the Log-demons DIR method outperformed the demons algorithm in terms of MI but underperformed compared to the affine registration for both eddy current and EPI distortions corrections. The absolute mean difference was decreased by 2.94%, 0.44%, and 1.53% compared to no correction, and affine, and

demons algorithm respectively when correcting for eddy current distortions, and decreased by 0.39%, 8.03%, and 13.19% compared to no correction, and affine, and demons algorithm respectively when correcting for EPI distortions.

Conclusion: This work indicates that the Log-Demons DIR algorithm is feasible to reduce eddy current and EPI distortions while preserving quantitative diffusion information. Although demonstrated with a DTI phantom study and brain study, this method could be extended for areas in which diffusion-weighted imaging is beneficial.

Contents

List of Tables

List of Figures

Acknowledgments

First, I would like to thank my research advisors, Drs Jim Chang and Dr. Fang Fang Yin, and my committee members, Dr. Junzo Chino and Dr. Oana Craciunescu for their guidance and support of my research and future endeavors.

I would also like to thank The Duke Cancer Institute for funding my research efforts.

Lastly, I would like to thank my family and friends, especially my parents, for their unconditional love and support in everything I do.

1. Introduction

Diffusion-Weighted (DW) magnetic resonance (MR) imaging provides image contrast that differs from conventional MR techniques by producing image contrast that is dependent on the molecular motion of water. Diffusion Tensor Imaging (DTI) is a powerful tool to characterize the magnitude, anisotropy, and orientation of the diffusion tensor. DTI is used to quantify three-dimensional (3D) spatial properties of water molecular diffusion processes, and as such probe tissue structure at a microscopic scale. Because DTI provides both anatomical and functional information it is a valuable tool to analyze the radiation-induced changes involved in radiation therapy treatments [2].

Because DW-MRI often uses a fast echo-planar imaging (EPI) technique, geometric distortions caused by susceptibility variation and eddy-currents are generally associated with diffusion-weighted images. Distortion correction is crucial to ensure an accurate analysis of the treatment response of radiation therapy.

1.1 MR Image Acquisition

Magnetic Resonance Imaging (MRI) is a non-ionizing imaging modality that takes advantage of the magnetic moments of protons within the body and their response to an external magnetic field [3]. MR signal is a small electric current induced in the receiving coil by the precession of the net magnetization of a region during resonance. The signal from the radio-frequency (RF) pulse has the form of either a free induction decay or echo. Voxels containing different materials have different spin densities and

relaxation times that produce different signal intensities. This difference in signal intensity. MR scanners can use differences in frequency, phase, and timing to localize information from each voxel that produces its own MR signal. In spin-echo imaging sequences, the repetition time (TR) and the echo time (TE) are manipulated to control the contrast of the MR image. The overall signal intensity of a spin-echo (SE) sequence can be expressed by:

$$S\alpha\rho_H\left[1 - e^{TR/T1}\right]e^{-TE/T2} \quad 1.1$$

For the purposes of this work, we will cover the relevant imaging sequences for this study.

1.1.1 T1 Weighted Imaging

A "T1" weighted SE sequence is designed to produce contrast principally based on the T1 characteristics of tissues. These images are achieved by using a short TR to maximize the differences in longitudinal magnetization recovery, and a short TE minimizes the T2 decay. The most intense signal in T1 weighted images is fat, followed by white matter, gray matter, and cerebral spinal fluid (CSF).

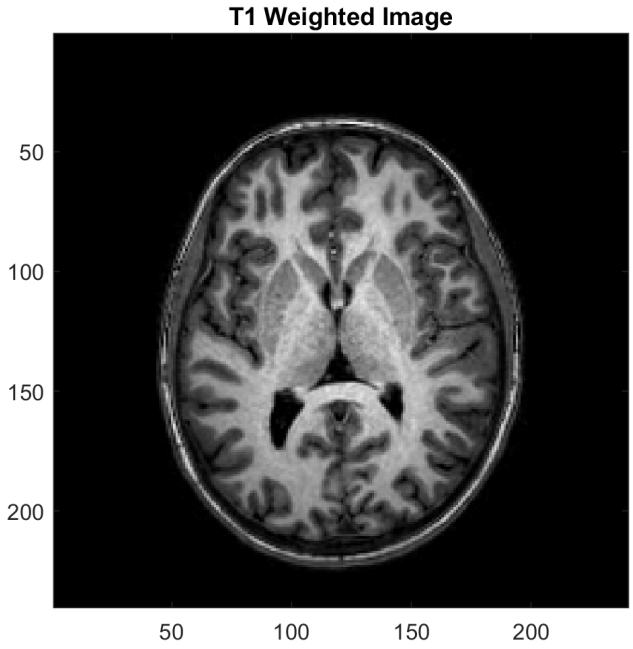

Figure 1.1: Representative image of an axial slice of T1 weighted brain scan

1.1.2 T2 Weighted Imaging

T2 weighted images utilize a long TR and TE to reduce T1 differences and emphasize the T2 differences. A T2 weighted image is often produced by an initial proton density-weighted echo followed by a second echo generated by a 180° of a long TR spin-echo pulse sequence. T2-weighted images have a higher tissue contrast compared to T1 weighted images.

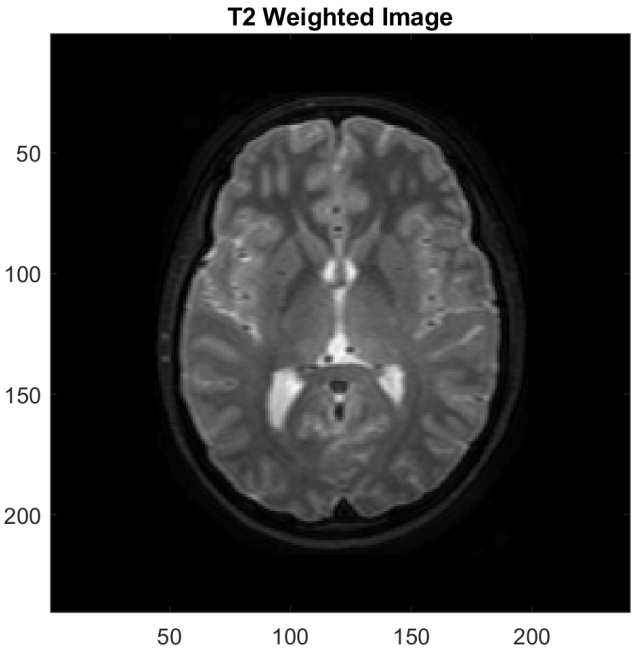

Figure 1. 2: Representative image of an axial slice of T2 weighted brain scan

1.1.3 Diffusion-Weighted Imaging

Diffusion relates to the random thermal motion of water molecules within a tissue. Cellular structures of different tissues produce varying anisotropic, directionally

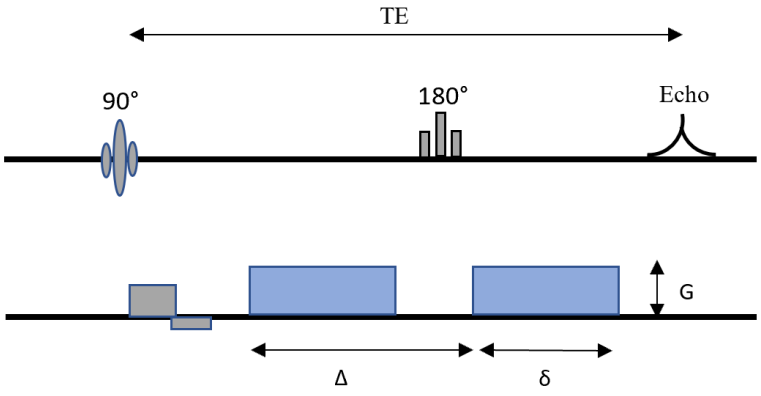

Figure 1.3 Pulse sequence diagram for DW acquisition showing that two diffusion gradients (blue) are added to either side of the refocusing pulse. The diffusion weighting factor, b. is dependent on the diffusion gradient amplitude(G), the duration of the diffusion gradient (δ), and the diffusion

dependent motion of water. Modern DWI techniques originate from the pulsed gradient spin echo (PGSE) technique develops by Stejskal and Tanner in 1964[4]. DWI sequences use two symmetric strong gradients on either side on the refocusing pulse to produce signal differences based on the restriction and directional of diffusion.

If enough time is allowed for diffusion, intracellular water motion may be restricted leading to a lower apparent diffusion coefficient (ADC) within a region of interest [5]. Diffusion-weighted contrast can be models by the exponential

$$S_i = S_0 \cdot e^{-b \cdot ADC_i} \quad 1.2$$

Where S_i is the DW signal intensity from a voxel within the diffusion-weighted image, S_0 is the signal intensity of the voxel without the diffusion sensitizing gradient applied, ADC_i is the apparent diffusion coefficient (described in section 1.2.1), and bis a factor that is determined by the strength, duration, and spacing of a rectangular gradient pulse and is represented by the equation,

$$b_{i,j} = \gamma^2 G_i G_j [\delta^2 (\Delta - \delta/3)] \quad 1.3$$

Where γ is the gyromagnetic ratio. The units of b are s/mm^2, which is reciprocal of the units of the ADC. A typical b-parameter strength is 1000s/mm^2. The ADC value relates to the rate of water diffusion within a tissue which also has an effect of the signal strength within a diffusion-weighted image [6] These sequences allow clinics to differentiate normal tissues from cancer and damaged tissue due to the differences in water mobility.

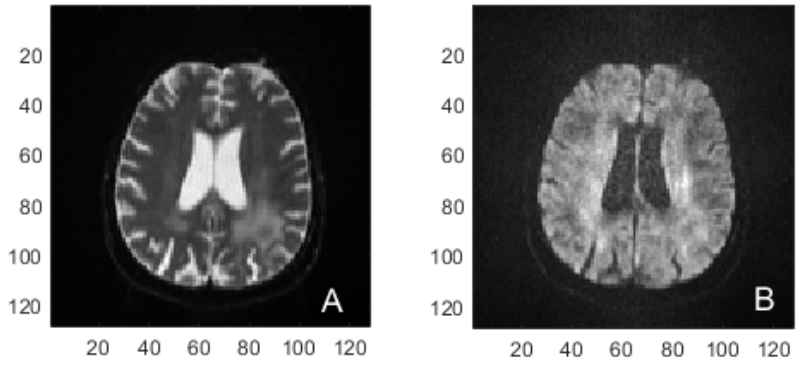

Figure 1.4: Representation of DWI images. Representative images of DWI images. Image A was acquired with an applied b-value of 0s/mm^2. Image B was acquired with an applied b-value of 1000s/mm^2

The clinical applications of DWI have shown promise in predicting and evaluating pathophysiology and is an indicator for early detection of ischemic injury. DWI and DTI are becoming useful tools to assess treatment response in radiation therapy.

1.2 Diffusion Tensor Imaging

Diffusion Tensor Imaging (DTI) is used often for the characterization of white matter (WM) in patients with brain lesions [7]. DTI maps help localize the white matter tracts that are important for critical functions such as motion, language, and vision that may be affected by the tumor or radiation therapy treatments [2][8].

Variations in diffusion-weighted signals due to the anisotropy of the region of interest can become an issue for clinical interpretation. For routine DWI acquisitions, the complexity is often ignored, and the ADC is taken as the single average value. If at least 6 diffusion encoding gradients are applied to the volume in noncollinear directions

along with a b=0s/mm^2 volume, the diffusion tensor can be calculated [6]. A diffusion tensor is a 2nd order tensor that models a 3D pattern of anisotropic diffusion within the region of interest. The diffusion tensor, D, can be determined by a variation of equation 1.2, in which you replace the ADC with D.

$$S = S_0 e^{\left(\Sigma_{i=x,y,z}\Sigma_{j=x,y,z} b_{i,j} D_{i,j}\right)} \quad 1.4$$

and equation 1.3 is replaced with

$$b_{i,j} = \gamma^2 G_i G_j [\delta^2(\Delta - \delta/3)] \quad 1.5$$

D corresponds to the diffusion rates in each combination of directions and is represented by

$$D = \begin{bmatrix} D_{xx} & D_{xy} & D_{xz} \\ D_{yx} & D_{yy} & D_{yz} \\ D_{zx} & D_{zy} & D_{zz} \end{bmatrix} \quad 1.6$$

The tensor is ideally symmetric and therefore the off-diagonal elements of the matrix are equal. The six elements, $\left(D_{xx}, D_{yy}, D_{zz}, D_{xy}, D_{xz}, D_{yz}\right)$, describe the ADC of water for each direction. A common way to conceptualize the diffusion tensor is through ellipsoids as shown in figure 1.5.

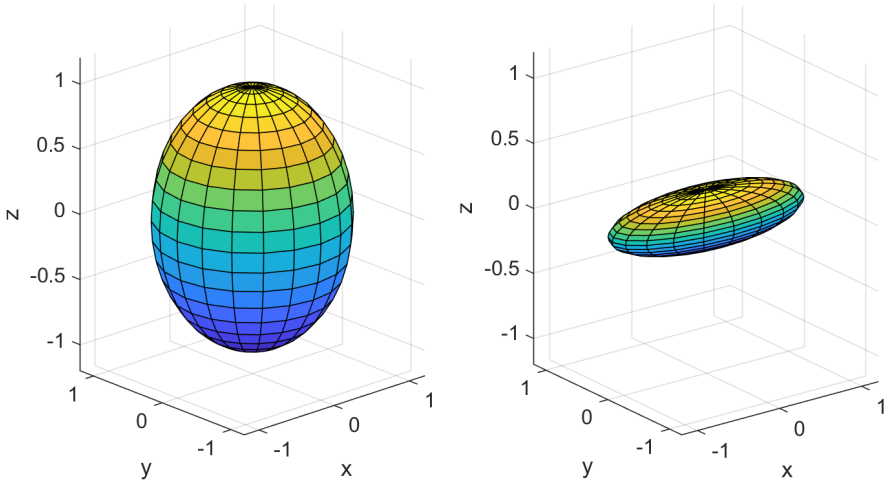

Figure 1.5: Representation of diffusion tensor ellipsoids. The figure on the left represents isotropic diffusion, while the ellipsoid on the right represents an anisotropic diffusion.

Diffusion tensor imaging (DTI) comprises a group of techniques where calculated eigenvalues ($\lambda_1, \lambda_2, and\ \lambda_3$) and eigenvectors ($\epsilon_1, \epsilon_2, and \epsilon_3$) are used to create images reflecting various diffusion properties of tissue. These eigenvectors can be calculated by diagonalizing D:

$$\Lambda = \begin{bmatrix} \lambda_1 & 0 & 0 \\ 0 & \lambda_2 & 0 \\ 0 & 0 & \lambda_3 \end{bmatrix} = R \cdot D \cdot R^T \qquad 1.7$$

The diffusion tensor is rotated by the matrix R whose columns are composed of the eigenvectors of the system and R^T is the transpose of the matrix R. The eigenvectors and eigenvalues describe the direction and lengths of the diffusion ellipsoid axes in descending order of magnitude. The primary eigenvector, ϵ_1 and its associated eigenvalue λ_1 designate the direction and magnitude of the greatest diffusion. The other

two eigenvectors are orthogonal to primary eigenvector and describe the radial diffusivity with a region[6][9]. Several rotationally invariant diffusion metrics can be calculated from the 3 eigenvalues and used to quantitatively track changes over time. The metrics called, "Diffusion Anisotropy Indices" (DAI) are single values that describe the microstructure within a voxel [6][7][9]. The DAIs can be visualized as seen in figure 1.6.

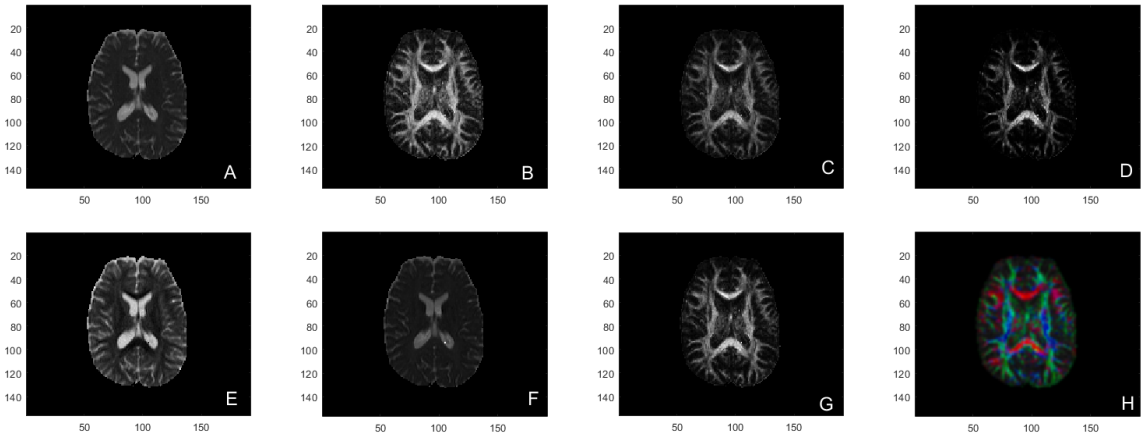

Figure 1.6: Top Row: A: The apparent diffusion coefficient map. B: The fractional anisotropy map. C: The relative Anisotropy Map. D: The volume fraction map. E: The axial diffusion map. F: The radial diffusion map. G: The lattice index map. H: The principal direction map

1.2.1 Apparent Diffusion Coefficient

The apparent diffusion coefficient (ADC) also referred to as the average diffusivity of the media can be calculated by taking the average of the eigenvalues [6][9][10].

$$ADC = \frac{\lambda_1 + \lambda_2 + \lambda_3}{3} = trace(D)/3 \qquad 1.8$$

Measurement of the ADC may help understand how the diffusivity is changing over time or after radiotherapy. A low signal within an image signifies restricted diffusion within a region of interest. ADC maps are particularly useful for detecting damaged areas of the brain after a stroke or within brain tumors as these areas typically have low diffusion.

1.2.2 Fractional Anisotropy

The Fractional Anisotropy (FA) is a dimensionless quantitative metric that measures the diffusion anisotropy or preferred direction of diffusion. The FA varies from 0 to 1, in which an FA of 0 represents isotropic diffusion while an FA of 1 represents perfectly linear diffusion. The FA measures the degree of directionality with a voxel:

$$FA = \frac{\sqrt{(\lambda_1 - \lambda_2)^2 + (\lambda_2 - \lambda_3)^2 + (\lambda_3 - \lambda_1)^2}}{\sqrt{2\sqrt{\lambda_1^2 + \lambda_2^2 + \lambda_3^2}}} \quad 1.9$$

and can also be related to the ADC by:

$$FA = \sqrt{\frac{3}{2}}\frac{\sqrt{(\lambda_1 - ADC)^2 + (\lambda_2 - ADC)^2 + (\lambda_3 - ADC)^2}}{\sqrt{2\sqrt{\lambda_1^2 + \lambda_2^2 + \lambda_3^2}}} \quad 1.10$$

1.2.3 Relative Anisotropy

Similar to the FA, the relative anisotropy (RA) also measures the diffusion asymmetry within a voxel and can be calculated by:

$$RA = \frac{\sqrt{(\lambda_1 - \lambda_2)^2 + (\lambda_2 - \lambda_3)^2 + (\lambda_3 - \lambda_1)^2}}{\lambda_1 + \lambda_2 + \lambda_3} \quad 1.11$$

and can also be related to the ADC by:

$$RA = \frac{\sqrt{(\lambda_1 - ADC)^2 + (\lambda_2 - ADC)^2 + (\lambda_3 - ADC)^2}}{\sqrt{2}\mathrm{ADC}} \quad 1.12$$

Both the FA and RA show different dependencies on $\lambda 1$, although the measure the same physical quantity [11].

1.2.4 D_{axial} & D_{radial}

The axial and radial diffusivity are metrics that provide directional information within a scan. As mentioned before the principal eigenvector and eigenvalue designate the direction and magnitude of greatest diffusion.

$$D_{axial} = \lambda_1 \quad 1.13$$

The radial diffusivity can be determined by the average of λ_2 and λ_3:

$$D_{radial} = (\lambda_2 + \lambda_3)/2 \quad 1.14$$

These values can be visualized by the axial diffusivity (D_{axial}). These values are used to demonstrate a more distinct relationship with the white matter tracts[7][12].

1.2.5 Lattice Index

In an attempt to mitigate noise, the lattice anisotropy index (LI), may be used. LI is an anisotropy index that is affected by the degree of orientational consistency[13][14]. The LI can be calculated by:

$$LI = (FA + FA^2)/2 \quad 1.15$$

1.2.6 Principal Diffusion Direction Map

The principal diffusion direction map assigns colors to voxels based on anisotropy and the primary direction. An RGB map is used to provide directional information and identify changes in WM tracts[6][7]. The typical convention is to have the principal eigenvector,ϵ_1, control the color and the FA to control the intensity. Red typically represents the left-right direction, green represents the anterior-posterior direction, and blue represents the superior-inferior direction.

2. Background

This chapter provides a literature review for the distortion corrections intrinsic to DWI and registration techniques intended to improve upon these distortions. A large number of publications are currently available, the papers were reviewed for the following registration techniques.

2.1 Distortions

2.1.1 EPI Distortions

Clinical DWI typically use single-shot EPI acquisitions that are sensitive to static magnetic field inhomogeneities, resulting in geometric distortions [15-20]. These distortions apply to all DWI and become more prominent with greater field strengths and appear pronounced along the phase encoding direction [15-20]. To be an effective tool in radiation therapy, EPI distortions need to be corrected before diffusion tensor calculation to accurately represent the anatomy and physiology within the image.

2.1.2 Eddy Current Distortions

Faraday-Lenz law states that electrical currents are induced in nearby conductors in a changing magnetic field [21]. Because DWI uses rapidly changing magnetic field gradients, eddy currents are induced in either the scanner or patient which warps the image and create two undesired occurrences: time-varying gradients and shifts in the main magnetic field (B_0). Eddy currents can result in higher ADC values along with geometric distortions. In diffusion-weighted EPI, eddy-current-induced gradients and

field shifts cause distinctive geometric distortions in the phase encoding direction of the resulting images [16,22-24]. Several techniques have been proposed to deal with eddy current distortions such as active shielding gradients [25], pre-emphasis currents and post-processing techniques[22]. For this study, we will be investigating several post-processing techniques.

2.2 Registration Methods

The classification of the registration method is dependent on the technique used. For our study, we measure the best transformation based on the squared error, cross-correlation, and mutual information between two images. Two categories of transformations are available to register images, rigid body model and deformable registration mode, but in this study, we chose to study the deformable registration techniques using the affine model, demons model and a Log Demons model [26,27].

2.2.2 Intensity-based Registration

Intensity-based image registration uses grayscale information to directly measure how well the two images are registered [28,29]. The registration is scored by a similarity measure, that determines the similarity between the distributions of voxel values from a static and transforming image. The common similarity measures used clinically are the sum of squared error(SE), cross-correlation (CC), and Mutual information (MI).

2.2.2.1 Sum of Squared Error

The squared error minimizes the sum of squares of the differences in intensity of images at corresponding pixel values.

$$SE = \sum_{i,j} \left(I_{i,j}^{moving} - I_{i,j}^{target} \right)^2 \quad 2.1$$

The standard error is a computationally simple calculation that minimizes the sum of squares of differences between the intensity of images at corresponding pixel values, which is represented by the $I_{i,j}$ variables for moving and target respectively. This method does have its limitations as it can only be used within the same imaging modalities.

2.2.2.2 Cross-Correlation

Another technique that has been used is the cross-correlation metric [29,30] that maximizes the correlation in the coincidence of image intensities. This method involves an assumption is that there is some linear relationship between the intensity values in the two images but may be used between dissimilar imaging modalities as long as the pixel intensities have the same relative order.

$$CC = \frac{\sum_i (x_i - \bar{\bar{x}})(y_i - \bar{\bar{y}})}{(\sum_i (x_i - \bar{\bar{x}})^2)^{1/2} (\sum_i (y_i - \bar{\bar{y}})^2)^{1/2}} \quad 2.2$$

Where x_i and y_i are the pixel values and $\bar{\bar{x}}$ and $\bar{\bar{y}}$ and the average pixel values of the moving and target images respectively.

2.2.2.3 Mutual Information

Mutual information maximizes the alignment of voxels whose values have common probabilities of being present in their respective image sets. MI can be used on images taken with dissimilar imaging modalities. Mutual information is particularly in radiation therapy because and MR acquisition may be able to better delineate the tumor but the CT is needed for dose calculation so MI is a common metric to register the two images [31].

$$MI(A,B) = \sum p_{AB}(i_a, j_b) \log_2 \left(\frac{p_{AB}(i_a, j_b)}{p_A(i_a) p_B(j_b)} \right) \quad 2.3$$

Where p_A is the probability distribution of the moving image (A), p_B is the probability distribution of the target image (B), and p_{AB} is the joint probability distributions of the moving and target images.

2.3 Geometric Models

Based on geometric models, registration techniques are broken down into two categories, Rigid Transformations and Deformable Registrations (non-rigid) [32], in which a transformation, T, will be applied to the moving image to align with a static image.

2.3.1 Rigid Transformations

2.3.1.1 Rigid Body

Rigid body registrations consist of a transformation involving three translation parameters and three rotation parameters.

2.3.1.2 Affine

Rigid body transformations can be expanded to 9 to 12 parameters to allow for affine registration by adding three scaling parameters and three shear parameters[29].

2.3.2 Deformable Registration

Deformable models have a different optimization criterion that is locally defined and computed and the deformation is constrained by a regularization term [33]. For this study, we focus on the demons and log demons deformable registration algorithms as described below.

2.3.2.1 Demons

The demons algorithm is based upon a thought experiment from James Clerk Maxwell in 1867 that suggested how the 2nd law of thermodynamics may be violated. Maxwell assumed a gas composed of two different particles and separated by a semi-permeable membrane that contains ”demons” that can differentiate the particles and allow them to diffuse in one direction. The ”demons” allow for unidirectional diffusion of the particles resulting in only blue particles in A and red particles in B.

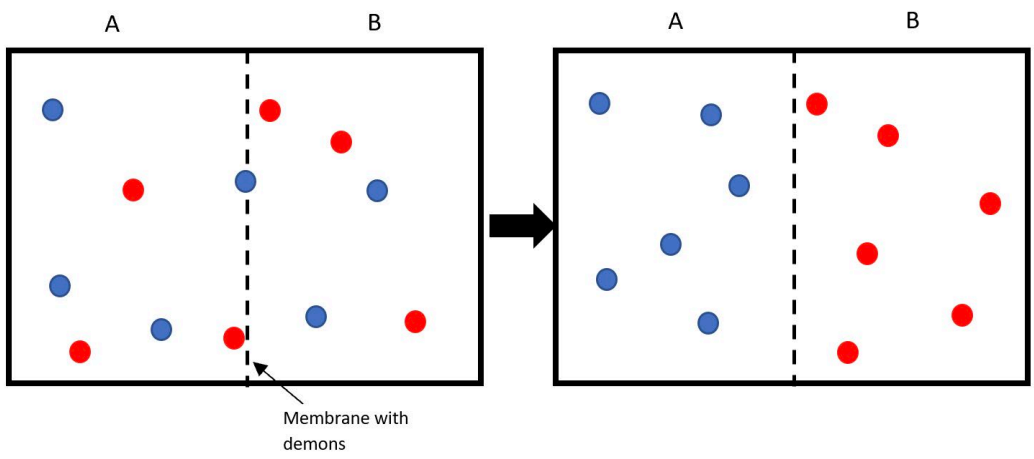

Figure 2.1: Depiction of Maxwell's demons thought experiment in which a mixed gas of red and blue particles separate themselves across the membrane with demons

Maxwell included the "demons" into the membrane to generate a greater amount of entropy to avoid any contradiction with the 2nd law of thermodynamics [34]. Thirion took this ideology and applied it to image registration to match a moving image to a target image by assuming the contour of an object in the moving image is the membrane, and "demons" are scattered along that membrane[34]. The relationship between the two images can be determined by the energy between them:

$$E(F, M, c, v) = \left\| \left(\frac{1}{\sigma_i} F - M \cdot c \right) \right\|^2 + \frac{1}{\sigma_x^2} dist(v, c) + \frac{1}{\sigma_T^2} Reg(v) \qquad 2.4$$

In which F is the fixed image, M is the moving image, σ_i accounts for the noise on the image intensity, σ_T^2 controls the amount of regularization, σ_x^2 accounts for the spatial

uncertainty and c is the non-parametric spatial transformation[34,35]. The regularization term, $Reg(v) = \left||\nabla v|\right|^2$ and the $dist(v,c) = \left||c - v|\right|$ are implemented to optimize the correlation between two images. The demons algorithm iteratively updates a displacement field, u by minimizing the energy with respect to u [34,35] which is applied to equation 2.4:

$$E_s^{corr} = \left||F - M \cdot v \cdot (Id + u)|\right|^2 + \frac{\sigma_i^2}{\sigma_x^2}\left||u^2|\right| \quad 2.5$$

Where s is the current transform and $s * (Id + \boldsymbol{u})$is a compositive adjustment.

2.3.2.2 Log-Demons

The demons registration has been improved upon by Vercauteren in which the diffeomorphic transformation is related to the exponential map of the velocity field, v [27,36]. Diffeomorphic demons registration can be extended to represent a total spatial transform in the log-domain. The algorithm takes the ongoing transformations as an exponential of a velocity field v. The log-domain demons algorithm uses Lie group structures to relate diffeomorphic transformation φ to the exponential of the velocity field[27][36][37]. The calculation of energy in equation 2.4 is modified to work in the log-domain by performing Gaussian smoothing in the log domain making $dist(s,c) = \left||log(s^{-1} \cdot c)|\right| and\ Reg(s) = \left||\Delta log(s)|\right|^2$. Using this equation 2.4 then becomes

$$E\big(F, M, exp(c), exp(v)\big) = \frac{1}{2\sigma_i^2}\Big(Sim\big(F, M \cdot \exp(c)\big) + Sim(F \cdot exp(-c), M)\Big)$$

$$+\frac{1}{\sigma_x^2} dist(c, v)^2 + \frac{1}{\sigma_T^2} Reg(v) \qquad 2.6$$

Where $\sigma_{x,T}^2$ control the step size and regularization and σ_i^2 controls the deformations of the image geometry[27,34,35].

2.3.3 Objectives of Thesis

The goal of this thesis is to evaluate Eddy-current distortion and EPI distortion corrections in the phase encoding direction in MR diffusion imaging using a log-demons DIR method with a phantom study and the massive dataset.

3. Correction of MR Distortions

3.1 Materials and Methods

Correction of eddy current distortions and EPI distortions using the log-demons algorithm involved taking advantage of different MR acquisition sequences. Because eddy current distortions are dependent on the strength and direction of the diffusion gradient [3,23,24,38], we take advantage of the fact that the $\boldsymbol{b = 0s/mm^2}$ images should not have any eddy-current distortions and only EPI distortions. T1 weighted images do not have any EPI distortions and are therefore used as an anatomical landmark when correcting these distortions. Registering the $\boldsymbol{b = 0s/mm^2}$ and $\boldsymbol{b = 1000s/mm^2}$ to the T1 weighted image would correct for any EPI and eddy-current distortions present. Here we describe several techniques to test the efficacy of the log-demons registration technique for its ability to preserve anatomical and functional information.

3.1.1 Diffusion Standard Model 128

In order to study the efficacy of the log-demons registration algorithm, we took Diffusion Standard Model 128 phantom[1] scans involving a T1 weighted scan, one $b = 0s/mm^2$ scan and twenty diffusion-weighted data sets with $b = 1{,}000s/mm^2$. The phantom's main components consist of 30mL vials of polymer in aqueous solution.

Figure 3.1: Depiction of the Diffusion Standard Model 128[1] phantom used to study the effects of eddy current and EPI distortions.

We rigidly register the T1 weighted image to the DWI, before applying any other registration technique to the images. For the diffusion tensor imaging (DTI) data set, slices were selected based on geometric landmarks and each registration algorithm was performed on the slices. A log-demons deformable registration algorithm was applied to a 2D slice and compared to affine and demons registration algorithms. Because these distortions mainly occur in the phase encoding direction, the transformations were only applied to the PE direction. The registered images were analyzed using mutual information (MI) for the algorithm's ability to correct eddy current and EPI deformations. The phantom contains thirteen vials of differing viscosity to study the differences in diffusion.

We tested the algorithms' ability to preserve information and image quality using the mean, and root mean square (RMS) for thirteen regions of interest (vials) in the Apparent Diffusion Coefficient (ADC) and Fractional Anisotropy (FA) maps.

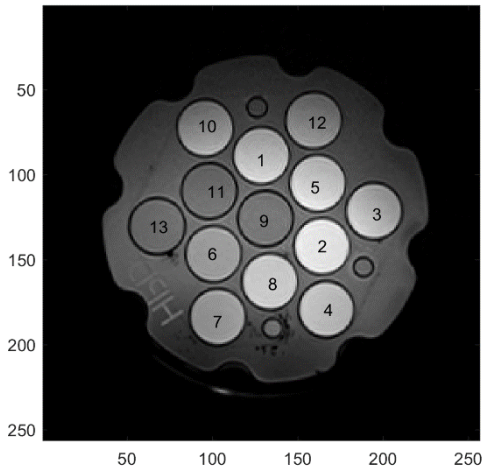

Figure 3.2: T1 weighted slice of the Diffusion phantom used with each of the vials numbered for reference.

3.1.2 MASSIVE dataset

The MASSIVE (Multiple Acquisitions for Standardization of Structural Imaging Validation and Evaluation) dataset [20] is a brain dataset of a single healthy patient consisting of 8000 diffusion-weighted MR volumes. We aim to expand upon our simplistic analysis of the performance of the log-demons algorithm using the diffusion phantom by using the MASSIVE data set. The MASSIVE data set provides diffusion-weighted volumes divided into four sets with both positive (+) and negative(-) diffusion gradient directions and both AP and PA phase encoding directions as seen in figure 7. To test the algorithms ability to correct eddy current distortions we register the AP+ and AP- $b = 1000s/mm^2$ images to the $b = 0s/mm^2$ image. A perfect registration/intensity correction algorithm would return identical image volumes after registering the distorted images to the b0

volume. We also compared the difference maps of the AP+ and AP- images after registration by the affine, demons, and log-demons algorithm. A similar technique is used to correct EPI distortions except the registrations were applied the AP+ and AP- $b = 0s/mm^2$ images to the T1-weighted image.

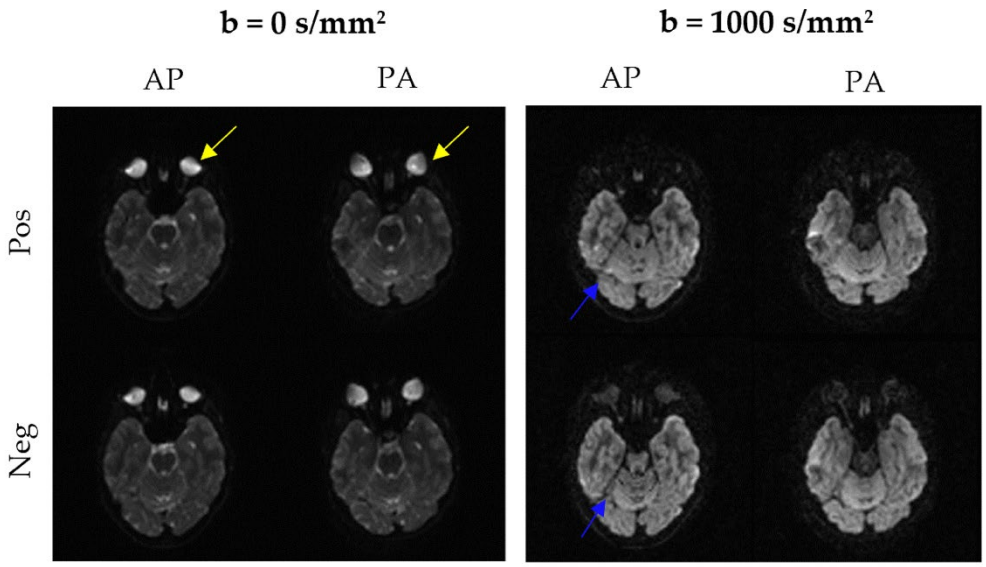

Figure 3.3: Representative images for the different sequences used in the MASSIVE dataset (AP+, AP-, PA+, PA-). The yellow arrow demonstrates the EPI distortions along the phase encoding direction present in the globes. The blue arrow demonstrates the intensity and shape of the changes due to eddy current distortions.

3.1.3 Methods

All image registration and diffusion tensor calculation are performed using MATLAB 2019a [39]. All registration algorithms were tested by correcting deformations in only the phase encoding direction.

4. Results

To validate the registration systems, three experiments were conducted using various datasets. The tests were conducted using MATLAB 2019a on a Dell XPS 15 9560 PC with a Windows 10 OS. The registration techniques demonstrated in this chapter are the affine registration, demons deformable registration, and log-demons deformable registration.

4.1 Phantom Study

4.1.1 Eddy Current Distortion

Correction for the eddy current distortions within the phantom involves registering the $b = 1000 s/mm^2$ to the $b = 0\ s/mm^2$ and analyzing using equations 2.1 – 2.3 to evaluate the similarity between the average of twenty 2D slices.

Table 1: Similarity measures for the eddy current distortion correction in the phase encoding direction

Correction Method	No correction	Affine PE	Demons PE	Log Demons PE
MSE	633740	634630	6.13E+05	620630
CC	0.7515	0.7518	0.6745	0.7523
MI	1.9976	2.0255	1.4961	2.0148

4.1.2 EPI Distortion

Correction for the eddy current distortions within the phantom involves registering the $b = 0\ s/mm^2$ to the T1-weighted image and analyzing using equations 2.1 – 2.3 to evaluate the similarity between the two images.

Table 2: Similarity measures for EPI Distortion correction in both the phase and frequency encoding direction

Correction Method	No correction	Affine PE	Demons PE	Log Demons PE
MSE	633740	634630	6.13E+05	620630
CC	0.8445	0.8054	0.8398	0.8737
MI	1.266	1.2609	1.2624	1.3429

4.1.3 Diffusion Tensor Analysis

The twenty $b = 1000s/mm^2$ slices were first registered to the $b = 0s/mm^2$ to remove eddy current distortions and then registered to the T1-weighted slice to correct any EPI distortions. The $b = 0s/mm^2$ slice was registered to the T1 weighted image to correct any EPI distortions. The ADC and FA were then calculated in MATLAB using the registered $b = 1000s/mm^2$ slices and $b = 0s/mm^2$ slice. Distortion correction and preservation of the images can be shown below in figure 4.1.

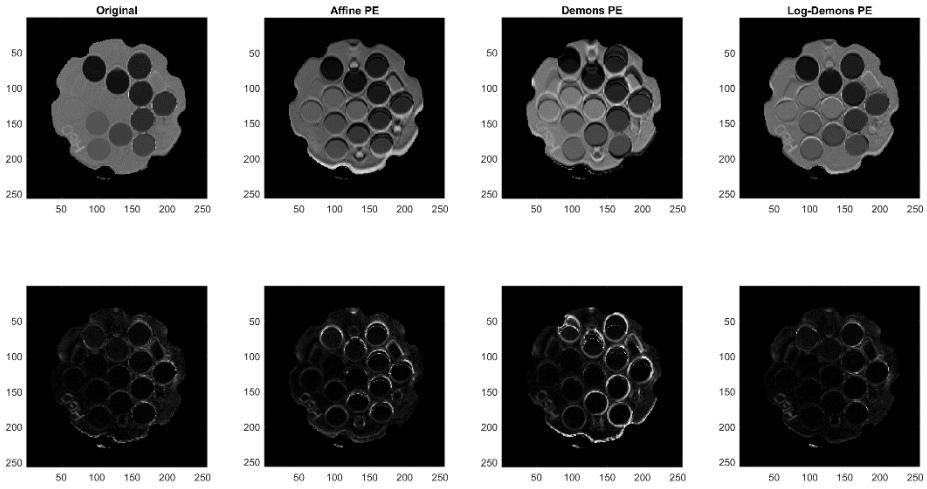

Figure 4.1: ADC (top) and FA(bottom)maps of the diffusion phantom to compare the integrity of the registration techniques in the phase encoding direction

The values were taken from each cylinder (see figure to determine similarity to the original ADC and FA image.

Table 3: ADC data from each of cylinder within the diffusion phantom for the images transformed in only the phase encoding direction in mm^2/s

	No Correction	Affine PE	Demons PE	Log-Demons PE
cylinder 1	0.001001	0.001069	0.001034	0.001000
cylinder 2	0.001386	0.001503	0.001366	0.001382
cylinder 3	0.000994	0.001024	0.001005	0.000995
cylinder 4	0.001816	0.001818	0.001805	0.001814
cylinder 5	0.001373	0.001357	0.001381	0.001375
cylinder 6	0.002259	0.002202	0.002294	0.002259
cylinder 7	0.000670	0.000613	0.001136	0.000670
cylinder 8	0.000669	0.000660	0.000763	0.000670
cylinder 9	0.001787	0.001756	0.001795	0.001787
cylinder 10	0.002268	0.002217	0.002327	0.002268
cylinder 11	0.002299	0.002258	0.002345	0.002298
cylinder 12	0.000417	0.000425	0.000711	0.000417
cylinder 13	0.000417	0.000381	0.000998	0.000415

Table 4: The average, standard deviation, and root mean squared error of the percent difference of the original ADC value in the phase encoding direction of the registered image

	Affine PE	Demons PE	Log- Demons PE
Average	3.73%	16.34%	1.75%
STD Dev	4.97%	27.37%	2.67%
RMS	4.83%	30.80%	2.58%

Table 5: FA data from each of cylinder within the diffusion phantom for the images transformed in only the phase encoding direction

	No Correction	Affine PE	Demons PE	Log Demons PE
cylinder 1	0.02168	0.04316	0.03378	0.02116
cylinder 2	0.02597	0.04905	0.03336	0.02587
cylinder 3	0.02304	0.03882	0.02978	0.02265
cylinder 4	0.02501	0.03241	0.02604	0.02468
cylinder 5	0.01966	0.03187	0.02144	0.01941
cylinder 6	0.01928	0.02054	0.02206	0.01884
cylinder 7	0.03867	0.06319	0.12093	0.03864
cylinder 8	0.03166	0.05189	0.05680	0.03130
cylinder 9	0.01889	0.01986	0.02005	0.01859
cylinder 10	0.02066	0.02075	0.02460	0.02048
cylinder 11	0.02093	0.02085	0.02685	0.02070
cylinder 12	0.04572	0.05342	0.09151	0.04546
cylinder 13	0.05380	0.06737	0.11925	0.05380

Table 6: The average, standard deviation, and root mean squared error of the percent difference of the original FA value in the phase encoding direction of the registered image

	Original	Affine PE	Demons PE	Log Demons PE
Average	0.00%	30.66%	36.20%	11.67%
STD Dev	0.00%	24.12%	30.82%	11.40%
RMS	0.00%	55.32%	60.17%	33.01%

4.2 MASSIVE Data

The massive data was implemented to test the log-demons algorithm's ability to correct DW distortions in brain scans. Three slices within the DWI volume were

randomly chosen and the affine, demons, and log-demons algorithms were applied to images in an attempt to correct for DWI distortions.

4.2.1 Eddy Current Distortion

To test the algorithm's ability to correct eddy current distortions, the AP+ and AP- b=1000s/mm^2 images were registered to the AP b = 0s/mm^2 image.

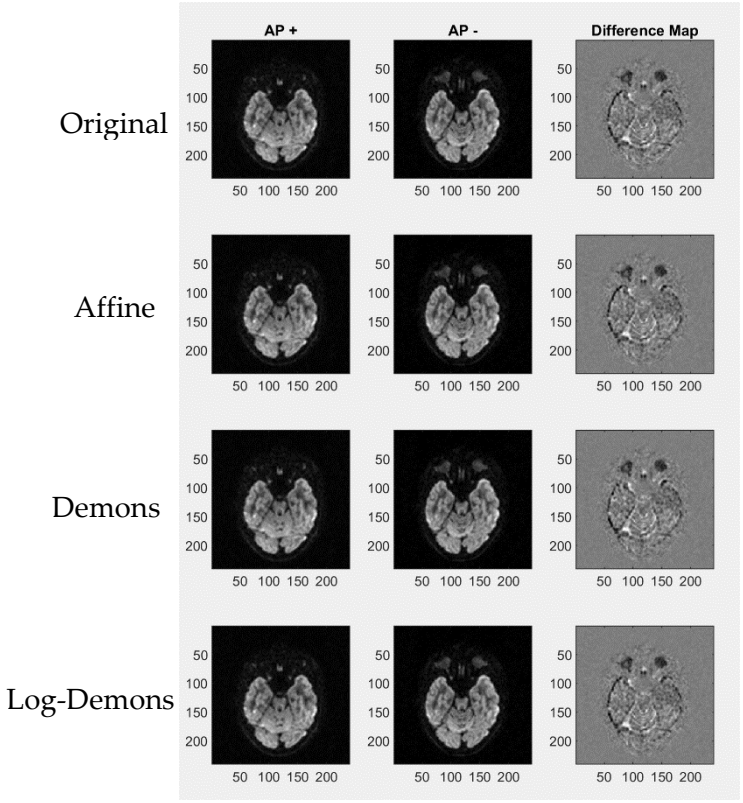

Figure 4.2: A representation of the DWI images and the difference map of the DWI images with opposing diffusion weighting gradients

Table 7: Mutual information from the corrected AP+ or AP- b=1000s/mm² image and b=0s/mm² image after correction applied along PE direction .

	Original	Affine PE	Demons PE	Log-Demons PE
Mutual Information	1.1373	1.1568	1.1433	1.1525

Table 8: The average absolute difference from corrected AP+ and AP- b=1000s/mm² image after correction applied along PE direction.

	Original	Affine PE	Demons PE	Log-Demons PE
Absolute Difference	38.4051	37.4424	37.8538	37.2936

4.2.2 EPI Distortion

To test the algorithm's ability to correct eddy current distortions, the AP+ and PA+ b=0s/mm² images were registered to the T1-weighted image.

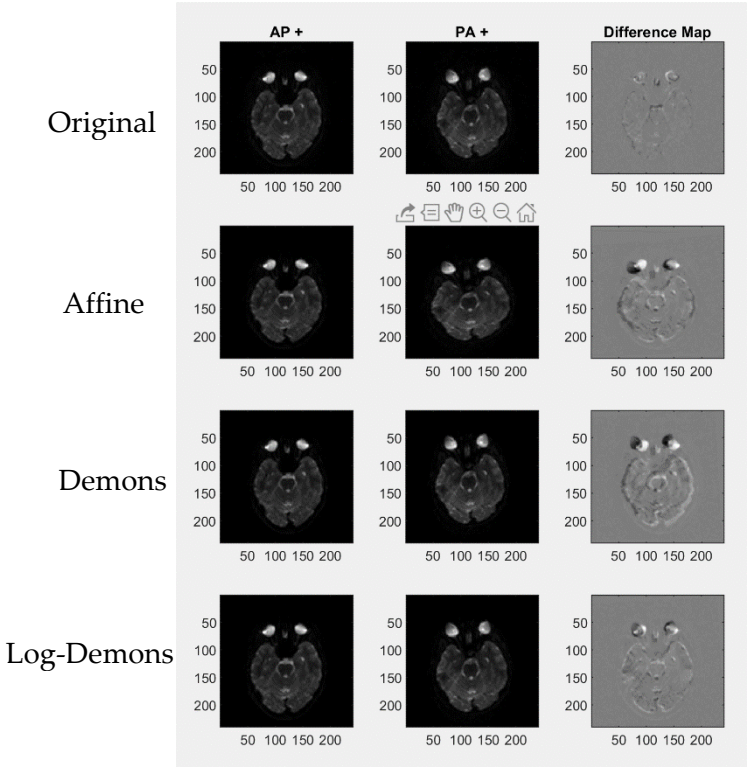

Figure 4.3: A representation of the registered b=0s/mm² images and the difference map of the DWI images with opposing diffusion weighting gradients

Table 9: Mutual information from the PE registered b=0s/mm² image and T1-weighted image.

	Original	Affine PE	Demons PE	Log-Demons PE
Mutual Information	0.8141	0.8661	0.8194	0.8193

Table 10: The average absolute difference from Corrected b=0s/mm² image and the T1-weighted image after correction applied along PE direction

	Original	Affine PE	Demons PE	Log-Demons PE
Absolute Difference	185.2624	200.6604	212.5919	184.5481

5. Discussion

5.1 Phantom Study

The log-demons algorithm has comparable results with the affine registration method that is commonly used to correct for eddy current distortions in diffusion imaging. As for the EPI distortion correction, the log demons algorithm more easily corrects larger scale deformations. The MI and CC were improved by, 2.15%, 0.89%, and 39.39% compared to no correction, affine, and demons algorithm respectively when correcting for eddy current distortions. MI and CC were improved by 8.89%, 9.33%, and 9.20% compared to no correction, and affine, and demons algorithm respectively when correcting for EPI distortions. This difference in effectiveness may be due to the algorithm's ability to contour the deformations. Because eddy current distortions are smaller in magnitude, the log-demons algorithm cannot accurately create the contour to show drastic improvement over the affine registration.

The log-demons algorithm outperformed both the affine and demons registration techniques in preserving diffusion tensor information as seen in tables 3-6 and figure 4.1. The average percent difference of the ADC and FA for the log-demons registration technique was substantially better for corrections in the phase encoding direction when compared to affine and demons registration techniques. Limiting the registration to the phase encoding direction yields a more accurate result, which is expected as both distortions primarily occur in the phase encoding direction.

Figures 4.1 and 4.2 provide a visualization of the performance of the algorithms. In the ADC images, the largest difference can be seen towards the edges of the cylinders and the phantom. As DWI becomes more prevalent in radiation oncology, distortion correction techniques will provide a better understanding of the anatomy and its function. The log-demons algorithm provides an image registration technique that can mitigate geometric and intensity distortions that affect the diffusion tensor. There is a noticeable difference in the affine and log-demons algorithms towards the bottom of the phantom. Preservation of the diffusion tensor imaging is especially important when examining regions undergoing radiation treatment to ensure any changes in the region are due to radiation and not caused by geometric deformations. Because the phantom is filled with water, we expect the diffusion to be fairly isotropic, which is why there is little signal from the FA maps. The FA maps of the affine and demons registered images are relatively brighter than the log-demons registered image. This visual analysis is a quick and simple method to ensure a deformation technique is preserving sensitive information. The diffusion phantom model 128 has provided a solid baseline in determining the efficacy of the log-demons algorithm and the rationale to apply these images to brain scans.

5.2 MASSIVE Data

The massive dataset provides useful information for benchmarking new algorithms involved in correcting eddy current and EPI distortions. The MASSIVE

dataset offers another metric to measure distortion corrections and an image registration's effectiveness. When correcting for EPI distortions, registering both the AP+ and AP- b=1000s/mm^2 images to a b=0s/mm^2 images the difference map of the two registered images provides a new metric to analyze distortion correction algorithms. An ideal correction would yield a zero-difference map. Surprisingly the algorithm that produced the highest MI did not yield the lowest average absolute difference.

When examining the EPI distortion corrections in tables 7 - 10 the log-demons algorithm improves the distortions as seen by the increase in MI and a decrease in average absolute difference. The average absolute difference decreased by 0.39%, 8.03%, and 13.19% compared to no correction, and affine, and demons algorithm respectively when correcting for EPI distortions. In figure 5.4 the difference map of the registration algorithms, the log-demons algorithm appears to have the least sharp contrast at the edges of the images. Through an assessment of the MI similarity metric and taking advantage of the physical principles of MR distortions, we are able to demonstrate the log-demons algorithm's ability to correct the eddy current distortions and EPI distortions intrinsic to DWI imaging. Although the algorithm has been shown to work in diffusion-tensor brain scans, the log-demons method could be extended for areas in which diffusion-weighted imaging is beneficial.

6. Conclusion

The research was focused on the development of a deformable registration algorithm to aid in the improvements of eddy current and EPI distortions without requiring an atlas. Using the log-demons algorithm and the similarity metrics, cross-correlation and mutual information we examined the log-demons algorithm to correct the distortions intrinsic to DTI, but also the preserve functional information DTI has to offer.

The proposed method allows for the correction of eddy current distortions and EPI distortions without requiring any preprocessing. By taking advantage of the log-demons ability to minimize the energy between two images and mitigate the distortions within the image. The algorithm outperformed the affine and demons registrations in correcting both eddy current and EPI distortions in the phase encoding direction and also preserving DTI information. When undergoing a study involving DTI analysis, measures should be taken to ensure that the information is being preserved if applying a transformation. The log-demons algorithm delivers an accurate correction for DTI that can provide a non-invasive measurement of treatment response. Although demonstrated with a DTI phantom study and the MASSIVE dataset, this method could be extended for areas in which diffusion-weighted imaging is beneficial.

This study may be limited in its structure as the MASSIVE dataset was taken with only one patient. Both the phantom study and MASSIVE dataset were acquired

using a smaller field of view when compared to other clinical DWI scans. Scans with a larger field of view have greater geometric distortions due to the non-linearity of the gradient applied in the phase encoding direction. To further strengthen the study, similar techniques may be applied to clinical brain scans to ensure the algorithm performs consistently across multiple patients. Further testing with scans involving a larger field of view may provide definitive evidence for the algorithm's performance.

References

[1] QalibreMD. Diffusion Standard Model 128 Diffusion Standard Model 128.(303):1–18, 2016.

[2] Zheng Chang, John P. Kirkpatrick, Zhiheng Wang, Jing Cai, Justus Adamson, and Fang Fang Yin. Evaluating radiation-induced white matter changes in patients treated with stereotactic radiosurgery using diffusion tensor imaging: A pilot study. Technology in Cancer Research and Treatment, 13(1):21–28, 2014.

[3] Jerrold T. Bushberg, J. Anthony Seibert, Edwin M. Leidholdt Jr., and John M.Boone.The Essential Physics of Medical Imaging. Lippincott Williams &Wilkins/Wolters Kluwer, Philadelphia, 3rd edition, 2012.

[4] E. O. Stejskal and J. E. Tanner. Spin diffusion measurements: Spin echoes in the presence of a time-dependent field gradient.The Journal of Chemical Physics,42(1):288–292, 1964.[5] Denis Le Bihan, Eric Breton, Denis Lallemand, Phillippe Grenier, EmmanuelCabanis, and Laval-Jeant. MR IMaging of Intravoxel Incoherent Motions: Ap-plications to Diffusion and Perfusion in Neurologic Disorders.Radiology, 161(2),1986.

[6] Pratik Mukherjee, J. I. Berman, S. W. Chung, C. P. Hess, and R. G. Henry.Diffusion tensor MR imaging and fiber tractography: Theoretical underpinnings.American Journal of Neuroradiology, 29(4):632–641, 2008.

[7] Andrew L Alexander, Jee Eun Lee, Mariana Lazar, and Aaron S Field.<Diffu-sion Tensor Imaging of the Brain- Alexander Leemans.pdf>.Neurotherapeutics,4(3):316–329, 2007.

[8] Brian P. Witwer, Roham Moftakhar, Khader M. Hasan, Praveen Deshmukh, Victor Haughton, Aaron Field, Konstantinos Arfanakis, Jane Noyes, Chad H.Moritz, M. Elizabeth Meyerand, Howard A. Rowley, Andrew L. Alexander, and Behnam Badie. Diffusion-tensor imaging of white matter tracts in patients with cerebral neoplasm.Journal of Neurosurgery, 97(3):568–575, 2002.

[9] Peter B. Kingsley. Introduction to diffusion tensor imaging mathematics: PartII. Anisotropy, diffusion-weighting factors, and gradient encoding schemes. 2006.29

[10] Qian Dong, Robert C. Welsh, Thomas L. Chenevert, Ruth C. Carlos, Pia Maly-Sundgren, Diana M. Gomez-Hassan, and Suresh K. Mukherji. Clinical Applications of Diffusion Tensor Imaging.Journal of Magnetic Resonance Imaging,19(1):6–18, 2004.

[11] Nikolaos G. Papadakis, Da Xing, Gavin C. Houston, Justin M. Smith, Mar-tin I. Smith, Michael F. James, Andrew A. Parsons, Christopher L.H. Huang,Laurance D. Hall, and T. Adrian Carpenter. A study of rotationally invariantand symmetric indices of diffusion anisotropy.Magnetic Resonance Imaging,17(6):881–892, 1999.

[12] Sheng Kwei Song, Shu Wei Sun, Michael J. Ramsbottom, Chen Chang, JohnRussell, and Anne H. Cross. Dysmyelination revealed through MRI as increasedradial (but unchanged axial) diffusion of water.NeuroImage, 17(3):1429–1436,2002.

[13] Konstantinos Arfanakis, Victor M. Haughton, John D. Carew, Baxter P. Rogers,Robert J. Dempsey, and M. Elizabeth Meyerand. Diffusion tensor MR imagingin diffuse axonal injury.American Journal of Neuroradiology, 23(5):794–802,2002.

[14] Carlo Pierpaoli and Peter J. Basser. Toward a quantitative assessment of diffu-sion anisotropy.Magnetic Resonance in Medicine, 36(6):893–906, 1996.

[15] Minjie Wu, Lin-Ching Chang, Lindsay Walker, Herve Lemaitre, Alan S. Barnett,Stefano Marenco, and Carlo Pierpaoli. Comparison of EPI Distortion CorrectionMethods in Diffusion Tensor MRI Using a Novel Framework. pages 321–329,2008.

[16] John C. Haselgrove and James R. Moore. Correction for distortion of echo-planar images used to calculate the apparent diffusion coefficient.MagneticResonance in Medicine, 36(6):960–964, 1996.

[17] Simon J Doran, Liz Charles-Edwards, Stefan A. Reinsberg, and Martin O Leach.A complete distortion correction for MR images: I. Gradient warp correction.Physics in Medicine and Biology, 50(7):1343–1361, 2005.

[18] Peter Jezzard and Robert S. Balaban. Correction for geometric distortion inecho planar images from B0 field variations.Magnetic Resonance in Medicine,34(1):65–73, 1995.

[19] Jeffrey Mark Treiber, Nathan S. White, Tyler Christian Steed, Hauke Bartsch,Dominic Holland, Nikdokht Farid, Carrie R. McDonald, Bob S. Carter, An-ders Martin Dale, and Clark C. Chen. Characterization and correction of ge-ometric distortions in 814 Diffusion Weighted Images.PLoS ONE, 11(3):1–9,2016.30

[20] Martijn Froeling, Chantal M.W. Tax, Sjoerd B. Vos, Peter R. Luijten, andAlexander Leemans. “MASSIVE” brain dataset: Multiple acquisitions for stan-dardization of structural imaging validation and evaluation.Magnetic Resonancein Medicine, 77(5):1797–1809, 2017.

[21] David J. Griffiths. Electromagnetic Induciton. InIntroduction to Electrodynam-ics, chapter 7. Electro, pages 319–324. Pearson Education, Upper Saddle River,NJ, third edition, 1999.

[22] William Spees, Niels Bul, Sun Peng, Joseph J.H Ackerman, Jefferey J. Neil, andJoel R. Garbow. Quantification and Compensation of Eddy-Current-InducedMagnetic Field Gradients.Journal of Magnetic Resonance, 212(1):116–123,2011.

[23] Jiancheng Zhuang, Jan Hrabe, Alayar Kangarlu, Dongrong Xu, Ravi Bansal,Craig A. Branch, and Bradley S. Peterson. Correction of eddy-current distor-tions in diffusion tensor images using the known directions and strengths ofdiffusion gradients.Journal of Magnetic Resonance Imaging, 24(5):1188–1193,2006.

[24] Peter Jezzard, Alan S. Barnett, and Carlo Pierpaoli. Characterization of andcorrection for eddy current artifacts in echo planar diffusion imaging.MagneticResonance in Medicine, 39(5):801–812, 1998.

[25] F. David Doty. MRI Gradient Coil Optimization.Spatially Resolved MagneticResonance., pages 647–674., 1998.

[26] Tom Vercauteren, Xavier Pennec, Aymeric Perchant, and Nicholas Ayache.Symmetric Log-Domain Diffeomorphic Registration. pages 1–8.

[27] Herve Lombaert, Leo Grady, Xavier Pennec, Nicholas Ayache, and FaridaCheriet. Spectral log-demons: Diffeomorphic image registration with very largedeformations.International Journal of Computer Vision, 107(3):254–271, 2014.

[28] M. L. Kessler. Image registration and data fusion in radiation therapy.BritishJournal of Radiology, 79(SPEC. ISS.):99–108, 2006.

[29] Kristy K. Brock, Sasa Mutic, Todd R. McNutt, Hua Li, and Marc L. Kessler.Use of image registration and fusion algorithms and techniques in radiother-apy: Report of the AAPM Radiation Therapy Committee Task Group No. 132:Report.Medical Physics, 44(7):e43–e76, 2017.

[30] Jeongtae Kim and Jeffrey A. Fessler. Intensity-Based Image Registration Us-ing Robust Correlation Coefficients.IEEE Transactions on Medical Imaging,23(11):1430–1444, 2004.31

[31] Frederik Maes, Andre Collignon, Dirk Vandermeulen, Guy Marchal, and PaulSuetens. Multimodality Image Registration by maximization of Mutual Infor-mation.IEEE TRANSACTIONS ON MEDICAL IMAGING, 16(2):187–198,1997.

[32] Derek L.G. Hill, Phillip G. Batchelor, Mark Holden, and David J Hawkes. Medical image registration.PHYSICS IN MEDICINE AND BIOLOGY, 46:R1–R45,2001.

[33] J. B.Antoine Maintz and Max A. Viergever. A survey of medical image regis-tration.Medical Image Analysis, 2(1):1–36, 1998.

[34] J. P. Thirion. Image matching as a diffusion process: An analogy with Maxwell'sdemons.Medical Image Analysis, 2(3):243–260, 1998.

[35] Tom Vercauteren, Xavier Pennec, Aymeric Perchant, and Nicholas Ayache. Dif-feomorphic demons: efficient non-parametric image registration.NeuroImage,45(1 Suppl):S61–S72, 2009.

[36] Tom Vercauteren, Xavier Pennec, Aymeric Perchant, and Nicholas Ayache.Symmetric Log-Domain Diffeomorphic Registration.edical Image Computingand Computer-Assisted Intervention – MICCAI 2008., 5241:1–8, 2008.

[37] Matias Bossa, Monica Hernandez, and Salvador Olmos. Contributions to 3DDiffeomorphic Atlas Estimation: Application to Brain Images.Medical ImageComputing and Computer-Assisted Interventions (MICCAI), 4791(June 2014),2007.

[38] M. Okan Irfanoglu, Joelle Sarlls, Amritha Nayak, and Carlo Pierpaoli. Evalu-ating corrections for Eddy-currents and other EPI distortions in diffusion MRI:methodology and a dataset for benchmarking. Magnetic Resonance in Medicine,81(4):2774–2787, 2019.

[39] MATLAB.9.6.0.1174912 (R2019a) Update 5. The MathWorks Inc., Natick,Massachusetts, 2019a.